DOI: https://doi.org/10.57233/ijsgs.v11i2.876 ISSNp: 2488-9229; ISSNe: 3027-1118

IJSGS FUGUSAU VOL. 11(2) WEBSITE: https://fugus-ijsgs.com.ng

INTERNATIONAL JOURNAL OF SCIENCE FOR GLOBAL SUSTAINABILITY
(A PUBLICATION OF FACULTY OF SCIENCE, FEDERAL UNIVERSITY GUSAU, NIGERIA)

Synthesis and Evaluation of Optical and Morphological Studies of Cu_2ZnSnS_4, Cu_2CoSnS_4 and Cu_2NiSnS_4 Thin Films using Chemical Bath Deposition Method for Device Applications

[1]J.E. Ekpe ,[1]N. M. Ekpe,[2]I. O. Alaekwe and [1]*C.N. Ukwu

[1]Department of Physics, Faculty of Physical Sciences, Alex Ekwueme Federal University Ndufu Alike, P.M.B. 1010, Ebonyi State, Nigeria
[2]Department of Chemistry, Faculty of Science, Federal University Gusau. Zamfara State. Nigeria

***Corresponding Author's Email& Phone No.:** nwalimondayekpe2019@gmail.com, +234837757081

Received on: April, 2025 **Revised and Accepted on:** May, 2025 **Published on:** July, 2025

ABSTRACT

Sustainable energy generation and conversion using kestrite solar cells are at the forefront of photovoltaic research interests. kesterites of Cu_2ZnSnS_4, Cu_2NiSnS_4 and Cu_2CoSnS_4, thin films were prepared on glass substrates using chemical bath deposition. The result showed that the absorbance of the thin films varied from 0.3 to 0.7 spanning the entire UV-VIS-NIR regions. The films showed high absorbance at a wavelength of 200nm and decreased exponentially to 400nm and gradually increased with increase in wavelength. The transmittance varied from 0-2% for Cu_2CoSnS_4, 0-2.3% for $Cu_2NiSnS4$ and 0-2.2% for Cu_2ZnSnS_4. The bandgaps of the films; 1.20 eV- 1.30 eV for Co^{2+}, 1.25 eV – 1.30 eV for Ni and 1.25eV-1.35eV for Zn^{2+} respectively. It was noticed that Zn^{2+}showed slight increase in the bandgap energies when compared to Co and Ni ion concentrations. Nevertheless, the ranges in the values of the energy gaps clearly showed that these thin films are very good materials for photovoltaic applications.Scanning electron micrographs result showed crystalline morphology for all the samples. The surface morphological study of Cu_2CoSnS_4, Cu_2NiSnS_4 and Cu_2ZnSnS_4 at (0.1M , 0.3M and 0.5M doping concentrations), showed that the grain size of all the samples are large and more oriented when doped with 0.5M and 0.3M concentration compared to that doped with 0.1M.

Keywords: Kesterites, Scanning electron micrograph, Perovskites, Transmittance, Doping

1.0 INTRODUCTION

Hybrid halide perovskites has attracted great research interests in the emerging thin film PV market. The search for higher power conversion efficiency thin film solar cells that will be stable and also made up of readily abundant materials is a continuous research interest in thin film fabrication or deposition.

For sustainable energy generation and conversions, kestrite solar cells are at the forefront of photovoltaic research interests. Devices based on the mineral kestrites could be the dark horse of next generation solar energy conversion (Walsh, 2017). Severe deficiencies in the availability and distribution of energy as a global commodity has been reported (Davis, et al 1995). There cannot be any meaningful development of any country without enough or abundant energy supply and its distribution. This is because energy is necessary and essential for various sectors of the economy of any country such as: health, processing industries, research institutes, schools and homes. Energy must be used in the provision of materials and services which are very vital for human existence such as: shelter, food, clothing, light, heat and transport. Thus presently, energy has become an integral part of people's daily life. No individual can be alive without the use of energy in one form or the other in any single day.

The electric energy (electricity) we use aresupplied to us from coal, petrol, and diesel. These energy sources are not environmentally friendly and in addition they are finite. In Nigeria, and other developing countries, there are very huge shortages of electricity.(world bank, 2021).

Efforts to use infinite or renewable energy sources such as solar radiation, wind and biomass energy are being intensified (Solanki, 2014). Renewable and non-renewable energy sources are the two broad categories of energy sources derived from the nature but have different perspective of availability (EIA, 2022). The rate of production of natural energy sources like petroleum, oil, natural gas and coal is low compared to the rate of consumption which is very high. Thus, the availability of the fossil fuels is limited and hence these fuels are regarded or classified as non- renewable energy sources. (DOE, 2023). On the other hand renewable energy sources are produced continuously by natural forces and processes that are present in environment. The renewable energy sources are biomass, solar radiation, hydro and wind. (IEA, 2023)

The main source of energy on the earth is the sun. We exist because of the energy from the sun, which reaches the earth in the form of electromagnetic radiation (NREL, 2022). The energy from fossil fuels are very small when compared to the energy that reaches the

DOI: https://doi.org/10.57233/ijsgs.v11i2.876 ISSNp: 2488-9229; ISSNe: 3027-1118

IJSGS FUGUSAU VOL. 11(2) WEBSITE: https://fugus-ijsgs.com.ng

earth from the sun. For instance, in 2010, the annual world energy consumption from all possible sources including electricity, coal, gas, diesel, petrol and biomass etc was 580 Exa joules while the availability of annual solar energy sources was 3,850,000 Exa joules (Solanki, 2014).

A solar cell converts photon power into electrical power and delivers this power to load, (Islam, 2006). Solar photovoltaic (PV) technology is a method of converting sunlight directly into electricity using semiconducting materials that exhibit the photovoltaic effect. (Green, 1982). This technology plays a crucial role in the shift toward clean, renewable energy and has widespread applications from small-scale devices to large power plants (IEA, 2021). The metal semiconductor (MS) junction cell, also called the Schottky-Queisser barrier cell has received much attention. In another development, the metal insulator – semiconductor (MIS) structures do offer very interesting new prospects for the development of thin film solar cells. (Starr and Palz, 1993).

The energy crisis has seriously increased, and search for high efficiency and low cost solar cells has become of great interest to energy industry likeCadium Indium Gallium Selenide (CIGS) solar cells (Mali, Patil, Betty, Devan, Ma, and Patil, 2012). Solar cells based on the kestertite mineral structure, including Cu_2ZnSnS_4 (CZTS), Cu_2ZnSe_4 ($CZTSS_e$), and thin alloys $Cu_2ZnSn(S_xSe_{1-x})_4$ ($CZTSS_e$), stand out from other thin film PV candidates for being composed of earth – abundant and nontoxic elements, (Walsh, 2017).

2.0 EXPERIMENTAL

Chemical bath deposition technique was used in this research to synthesize the kesterites such as Cu_2ZnSnS_4, Cu_2NiSnS_4 and Cu_2CoSnS_4. This was done by depositing these kesterites thin film on plane glass substrates. The microscopic glass slide (substrates) prior to the deposition was degreased by soaking them in the concentrated hydrochloric acid for about 2 hours. At the expiration of this period, the substrates were removed and washed with foam-sponge in ethanol and detergent solution. At the end of this process, the substrates were rinsed in distilled water and left to dry in dust-free environment.

The experiment set up was arranged in such way that the cations and anionssource were mixed in the beaker and used for the deposition in order of adsorption reactions. The beaker contains the mixed cationic precursor solution and anion in the ratio of (1:1:1). Each of Cu_2CoSnS_4, Cu_2NiSnS_4 and Cu_2ZnSnS_4 has a volume of 25ml which gives a total of 75ml. The beaker was placed inside a heating water bath that was set at 70^0C and it was left for about 6 hours under constant check of the temperature. After 6 hours the glass substrate was removed and rinsed with the de-ionized water of volume 80ml to remove the loosely adsorbed cation and anion from the substrate.

The anionic precursor: 0.3M thioacetamide ($C_2H_5N_2S$) solution which served as source of sulphur and 2ml (NH_4) was used as complexing agents. The beakers were kept at constant temperature 70°C. The pH values of the cationic and anionic precursors were 3 and 6 respectively before mixing the solutions together. The well cleaned substrates were dipped in the beakers containing cationic and anionic precursors of Cu^+, Co^+, Zn^{2+}, Ni^+, Sn^{2+} and S^{2-} that get adsorbed on substrate surface.

3.0 RESULTS

3.1. The results of optical and solid state properties such as absorbance, transmittance, reflectance, energy band gap, extinction coefficient, refractive index, real and imaginary parts of dielectric constant including optical conductivity of Cu_2CoSnS_4, Cu_2ZnSnS_4 and Cu_2NiSnS_4 thin films are shown below.

3.1.1 Absorbance**:** Figures 1-3, Absorbance Vs Wavelength for Cu_2CoSnS_4, Cu_2ZnSnS_4 and Cu_2NiSnS_4 at 0.1M, 0.2M, 0.3M, 0.4M and 0.5M

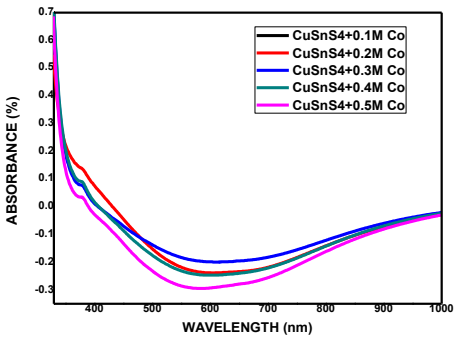

Fig. 1 Absorbance Vs Wavelength for Cu_2CoSnS_4 at 0.1M, 0.2M, 0.3M, 0.4M and 0.5M 0.

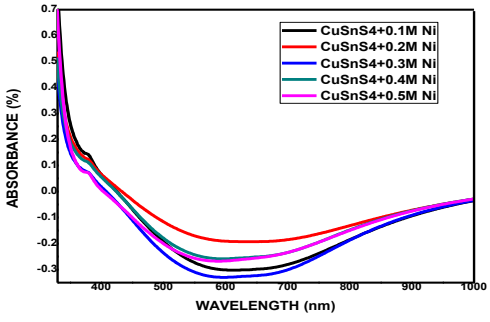

Fig. 2: Absorbance Vs Wavelength for Cu_2NiSnS_4 at 0.1M, 0.2M, 3M, 0.4M and 0.5M

DOI: https://doi.org/10.57233/ijsgs.v11i2.876 ISSNp: 2488-9229; ISSNe: 3027-1118

IJSGS FUGUSAU VOL. 11(2) WEBSITE: https://fugus-ijsgs.com.ng

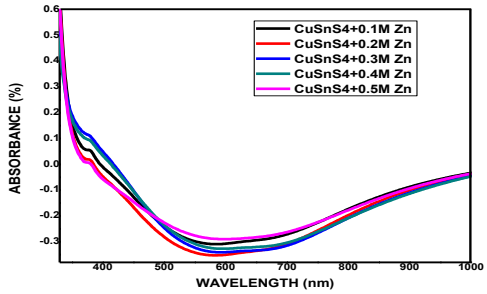

Fig.3 Absorbance Vs Wavelength for Cu_2ZnSnS_4 @ 0.1M, 0.2M, 0.3M, 0.4M and 0.5M

3.1.2. TransmittancE**:** Figures 4-6, Transmittance Vs Wavelength for Cu_2CoSnS_4, Cu_2ZnSnS_4 and Cu_2NiSnS_4 at 0.1M, 0.2M, 0.3M, 0.4M and 0.5M

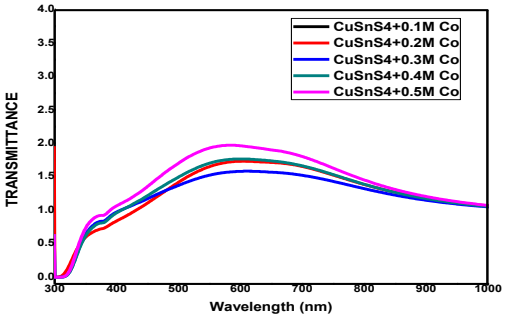

Fig.4: Transmittance Vs Wavelength for Cu_2CoSnS_4 at 0.1M, 0.2M, 0.3M, 0.4M and 0.5M

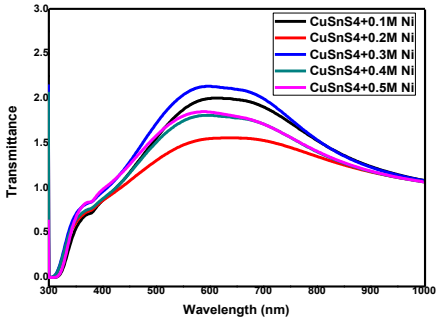

Fig.5 Transmittance Vs Wavelength for Cu_2NiSnS_4 at 0.1M, 0.2M, 0.3M, 0.4M and 0.5

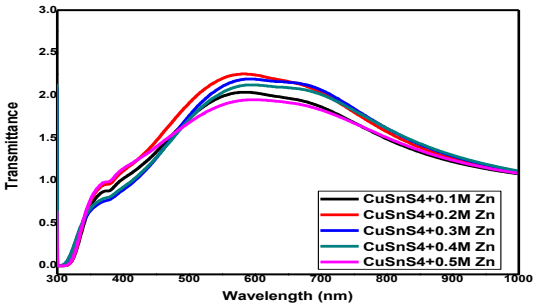

Fig. 6 Transmittance Vs Wavelength for Cu_2ZnSnS_4 at 0.1M, 0.2M, 0.3M, 0.4M and 0.5M

3.1.3 Reflectance: Figures 7-9, Reflectance Vs Wavelength for Cu_2CoSnS_4, Cu_2ZnSnS_4 and Cu_2NiSnS_4 at 0.1M, 0.2M, 0.3M, 0.4M and 0.5M

DOI: https://doi.org/10.57233/ijsgs.v11i2.876 ISSNp: 2488-9229; ISSNe: 3027-1118

IJSGS FUGUSAU VOL. 11(2) WEBSITE: https://fugus-ijsgs.com.ng

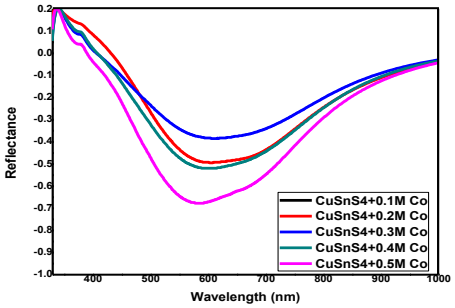

Fig.7: Reflectance Vs Wavelength for Cu_2CoSnS_4 at 0.1M, 0.2M, 0.3M, 0.4M and 0.5M

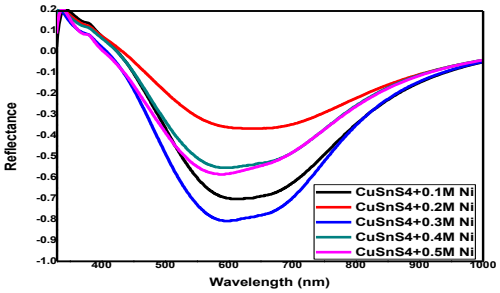

Fig.8: Reflectance Vs Wavelength for Cu_2NiSnS_4 at 0.1M, 0.2M, 0.3M, 0.4M and 0.5M

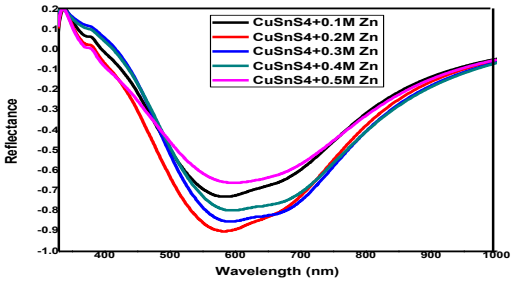

Fig.9: Reflectance Vs Wavelength for Cu_2ZnSnS_4 at 0.1M, 0.2M, 0.3M, 0.4M and 0.5M

3.1.4 Band gap Energy**:** Figures 10 – 12, $(\alpha hv)^2$ (eV^2m^{-2}) Vs hv(eV) for Cu_2CoSnS_4, Cu_2ZnSnS_4 and Cu_2NiSnS_4 at 0.1M, 0.2M, 0.3M, 0.4M and 0.5M

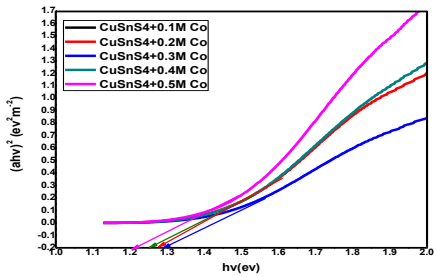

Fig. 10: $(\alpha hv)^2$ (eV^2m^{-2}) Vs hv(eV) for Cu_2CoSnS_4 at 0.1M, 0.2M, 0.3M, 0.4M and 0.5M

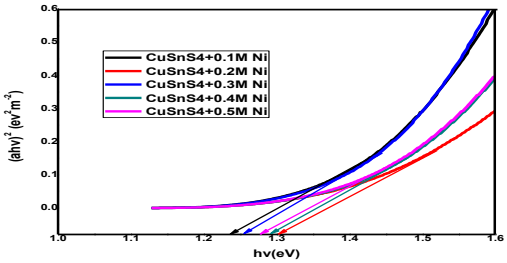

Fig.11: $(\alpha hv)^2$ (eV^2m^{-2}) Vs hv(eV) for Cu_2NiSnS_4 at 0.1M, 0.2M, 0.3M, 0.4M and 0.5M

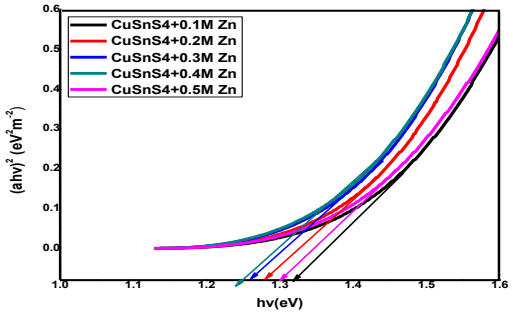

Fig.12: $(\alpha hv)^2$ (eV^2m^{-2}) Vs hv(eV) for Cu_2ZnSnS_4 at 0.1M, 0.2M, 0.3M, 0.4M and 0.5M

4.1.5 Refractive Index**:** Figures 13 – 16 show plot of Refractive index (n) Vs hv (eV) for Cu_2CoSnS_4, Cu_2ZnSnS_4 and Cu_2NiSnS_4 at 0.1M, 0.2M, 0.3M, 0.4M and 0.5M

DOI: https://doi.org/10.57233/ijsgs.v11i2.876 ISSNp: 2488-9229; ISSNe: 3027-1118

IJSGS FUGUSAU VOL. 11(2) WEBSITE: https://fugus-ijsgs.com.ng

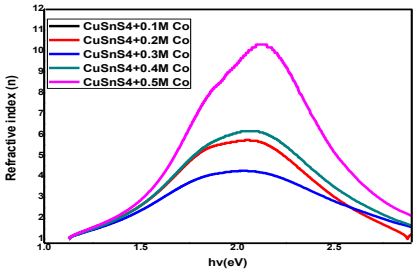

Fig. 13: Refractive index (n) Vs hv(eV) for Cu_2CoSnS_4 at 0.1M, 0.2M, 0.3M, 0.4M and 0.5M

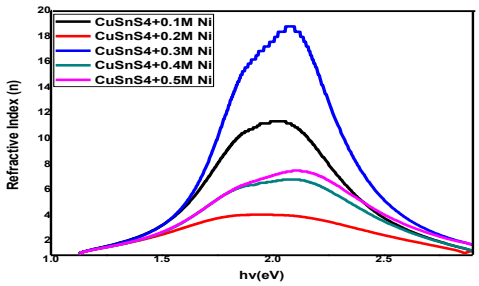

Fig. 14: Refractive index (n) Vs hv(eV) for Cu_2NiSnS_4 at 0.1M, 0.2M, 0.3M, 0.4M and 0.5M

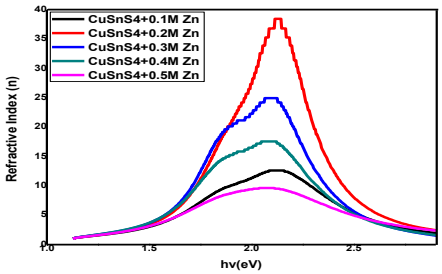

Fig.16: Refractive index (n) Vs hv(eV) for Cu_2ZnSnS_4 at 0.1M, 0.2M, 0.3M, 0.4M and 0.5M

4.1.6 Extinction Coefficient**:** The plots of Extinction coefficient (k) against Photo energy are displayed in figures 17 to 19

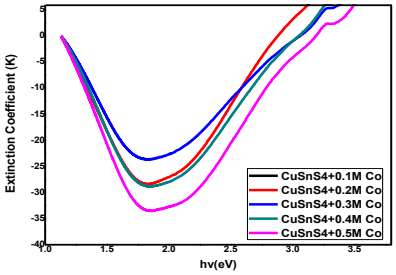

Fig.17: Extinction Coefficient Vs hv(eV) for Cu_2CoSnS_4 at 0.1M, 0.2M, 0.3M, 0.4M and 0.5M

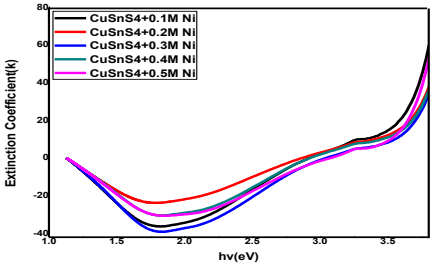

Fig. 18: Extinction Coefficient Vs hv(eV) for Cu_2NiSnS_4 at 0.1M, 0.2M, 0.3M, 0.4M and 0.5M

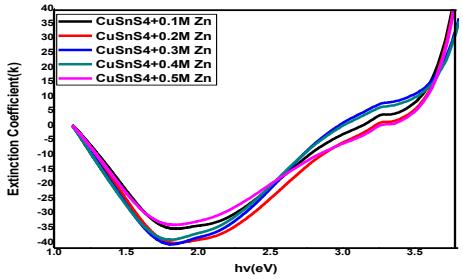

Fig. 19: Extinction Coefficient Vs hv(eV) for Cu_2ZnSnS_4 at 0.1M, 0.2M, 0.3M, 0.4M and 0.5M

4.1.7. Optical Conductivity:Figures 20 – 22, show the plots of Optical conductivity against Photon energy for the different thin films deposited in this work

DOI: https://doi.org/10.57233/ijsgs.v11i2.876 ISSNp: 2488-9229; ISSNe: 3027-1118

IJSGS FUGUSAU VOL. 11(2) WEBSITE: https://fugus-ijsgs.com.ng

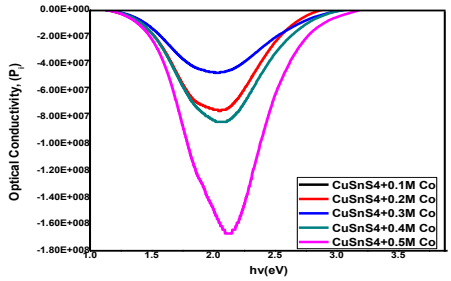

Fig.20: Optical Conductivity Vs hv(eV) for Cu_2CoSnS_4 at 0.1M, 0.2M, 0.3M, 0.4M and 0.5M

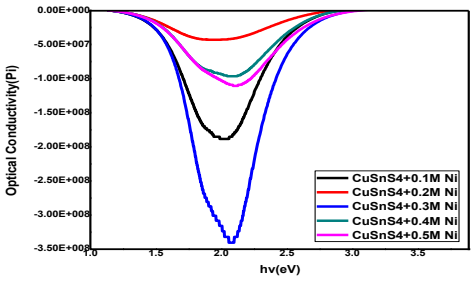

Fig. 21: Optical Conductivity Vs hv(eV) for Cu_2NiSnS_4 at 0.1M, 0.2M, 0.3M, 0.4M and 0.5M

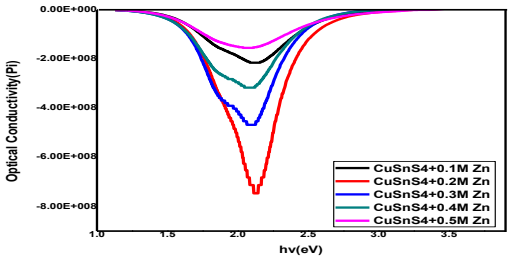

Fig. 22: Optical Conductivity Vs hv(eV) for Cu_2ZnSnS_4 at 0.1M, 0.2M, 0.3M, 0.4M and 0.5M

4.1.8 Dielectric Constant Real) ε_r **:** Figures 23 – 25, show the plots of Dielectric constant against Photon energy for the different thin films deposited in this work

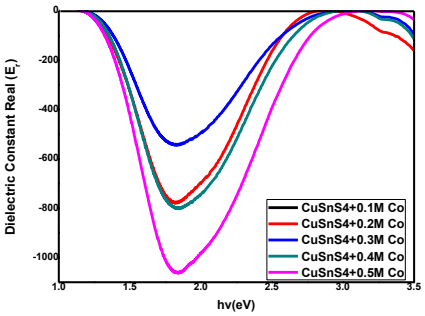

Fig.23: Dielectric const. (ε_r) Vs hv(eV) for Cu_2CoSnS_4 at 0.1M, 0.2M, 0.3M, 0.4M and 0.5M

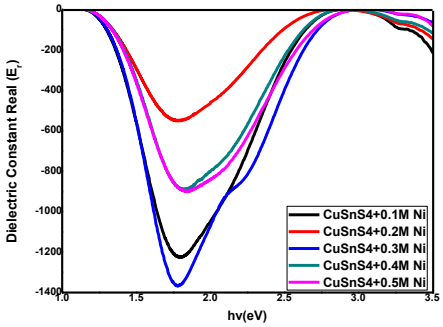

Fig.24: Dielectric const. (ε_r) Vs hv(eV) for Cu_2NiSnS_4 at 0.1M, 0.2M, 0.3M, 0.4M and 0.5M

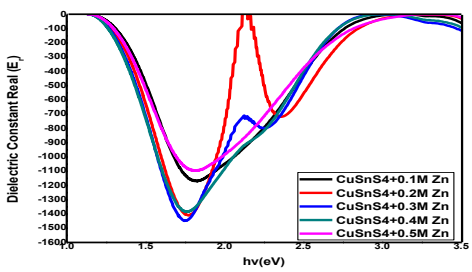

Fig.25: Dielectric const. (ε_r) Vs hv(eV) for Cu_2ZnSnS_4 at 0.1M, 0.2M, 0.3M, 0.4M and 0.5M

DOI: https://doi.org/10.57233/ijsgs.v11i2.876 ISSNp: 2488-9229; ISSNe: 3027-1118

IJSGS FUGUSAU VOL. 11(2) WEBSITE: https://fugus-ijsgs.com.ng

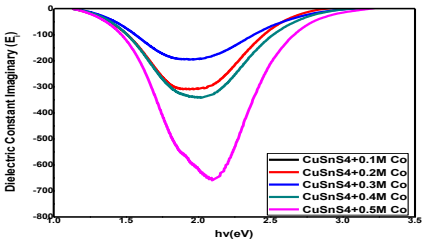

4.1.9 Dielectric Constant (imaginary) **εi:**Figures 28, show the plots of Dielectric constant (imaginary)against Photon energy for the different thin films deposited in this work

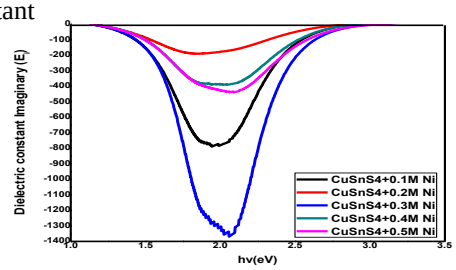

Fig.26: Dielectric const. (εi) Vs hv(eV) for Cu_2CoSnS_4 at 0.1M, 0.2M, 0.3M, 0.4M and 0.5M

Fig.27: Dielectric const. (εi) Vs hv(eV) for Cu_2NiSnS_4 at 0.1M, 0.2M, 0.3M, 0.4M and 0.5M

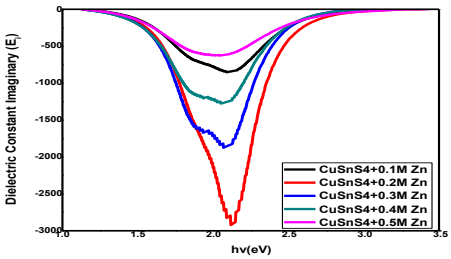

Fig.28: Dielectric const. (εi) Vs hv(eV) for Cu_2ZnSnS_4 at 0.1M, 0.2M, 0.3M, 0.4M and 0.5M

4.2: Structural Analysis**:** The SEM images of Cu_2SnS_4 doped with Co, Ni and Zn shown in figures 29 – 34below

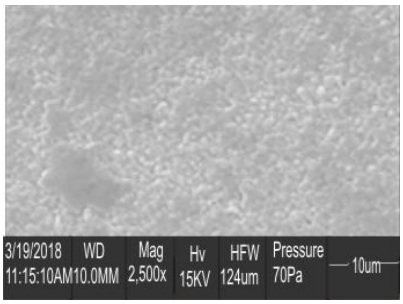

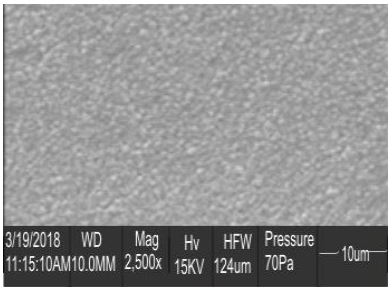

Fig. 29: Sem image of Cu_2SnS_4 doped with 0.1M of Co

Fig. 30: Sem image OF Cu_2SnS_4 doped with 0.3M of Co

DOI: https://doi.org/10.57233/ijsgs.v11i2.876 ISSNp: 2488-9229; ISSNe: 3027-1118

IJSGS FUGUSAU VOL. 11(2) WEBSITE: https://fugus-ijsgs.com.ng

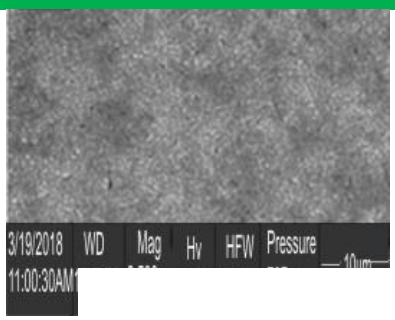

Fig. 31: Sem image of Cu_2SnS4 doped with 0.5M of Co

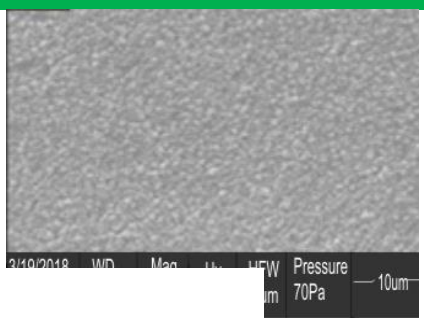

Fig. 32: Sem image of Cu_2SnS_4 doped with 0.3M of Ni

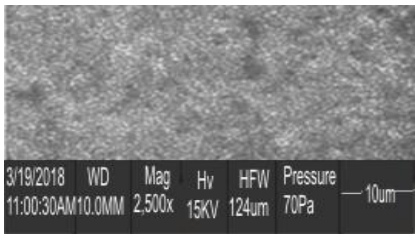

Fig. 33: Sem image of Cu_2SnS_4 doped with 0.5M of Ni

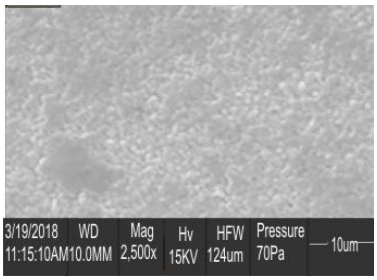

Fig. 34: Sem Image of Cu_2SnS_4 doped with 0.1m zn

4.3: X-ray diffraction (XRD) Pattern:The XRD patterns of the deposited films are shown in figures 35- 37 below

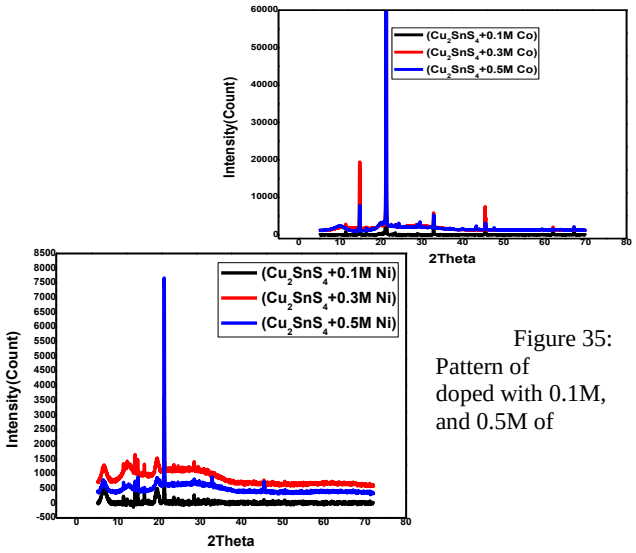

Figure 35: XRD Pattern of **Cu_2SnS_4** doped with 0.1M, 0.3M, and 0.5M of **Ni**

Figure 36: XRD Pattern of Cu_2SnS_4 doped with 0.1M, 0.3M, and 0.5M of Ni

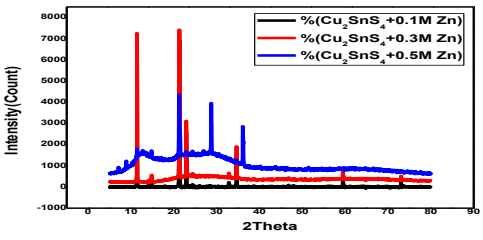

XRD **Cu_2SnS_4** 0.3M, Co^{2+},

Figure 37: XRD Pattern of Cu_2SnS_4 doped with 0.1M, 0.3M, and 0.5M of Zn^{2+},

4.0 DISCUSSION OF RESULTS

4.1 Optical and Solid State Analysis

The optical and solid state properties of the thin films deposited are discussed below

4.1.1 Absorbance

The plot of absorbance against wavelength is shown in Fig (1-3) for Cu_2CoSnS_4, Cu_2NiSnS_4 and Cu_2ZnSnS_4 with different doping concentrations of Co, Ni and Zn respectively. The graph of thin films showed clearly

DOI: https://doi.org/10.57233/ijsgs.v11i2.876 ISSNp: 2488-9229; ISSNe: 3027-1118
IJSGS FUGUSAU VOL. 11(2) WEBSITE: https://fugus-ijsgs.com.ng

that the three films have a greater absorbance in the visible region of electromagnetic spectrum. The plot also showed that the absorbance decreased with increase in wavelength and doping concentrations, which followed similar trend exhibiting a maximum in the visible region and minimum in the UV region. The absorbance varies from 0.3 to 0.7 spanning the entire UV-VIS-NIR regions. The films show high absorbance at a wavelength 200 nm and falls exponentially to 400 nm and gradually increase with increase in wavelength. The result indicates that as the concentration of the dopant increases, the absorbance increases which is in agreement with the XRD analysis. When doped with Ni, this optical behavior showed that we can tune the optical properties to suit a specific application by varying growth parameters. This property of highest absorbance in the UV region makes the films good materials for the construction of poultry roofs and walls to warm the inside of the poultry house which is needed by the young chicks. It could also be used for coating of the eyeglasses for protection of the skin around the eye. The calculated absorption spectra are compared with the experimental spectra measured at room temperature, which reveals photo-absorption in the entire visible region with very high absorption coefficient $\alpha > 10^5$ cm^{-1}. (Sachin*et al*, 2017). (Maarja *etal* (2019) reported absorption coefficient of ~10cm^{-1} for $Cu_2ZnSn(S_xSe_{1-x})_4$.

4.1.2 Transmittance

The transmittance is generally low compared to reported values of 85% for ZnS by (Jinhuo and Wenjian, 2014). The plot of transmittance against wavelength is shown in figure (8-10) for Cu_2CoSnS_4, Cu2NiSnS4and Cu_2ZnSnS_4 with different doping concentrations of Co, Ni and Zn respectively. The transmittance value for all the deposited thin films increases with increasing wavelength from 200 nm to 600 nm and decreases from 700 nm to 1000 nm.
The films show high transmittance at visible region to near infra red region and low transmittance at the ultra violet region with the five layers from each plot recording

Maximum transmittance in the visible region to near infra red region and minimum in the UV region. The transparency generally varies from 0-2%, 0-2.3% and 0-2.2% for Cu_2CoSnS_4, $Cu_2NiSnS4$and Cu_2ZnSnS_4 respectively.

The deposition conditions may be responsible for this optical behavior. The plots in Fig (4-6) also show that doping concentrations enhances the transmittance of the films and are in trend. From the transmission spectra it is observed that the film samples transmittance clearly within VIS-NIR regions but moderately in the UV regions. The as-deposited sample has maximum transmittance of about 78 %while the maximum transmittance for the samples doped with Co, Ni and Zn are 80 %, 75 % and 65 % respectively. All the film samples showed transmittance that increased exponentially from the UV region towards the NIR region. The properties of moderately high transmittance in the VIS-NIR exhibited by film samples make the films good material for coating of poultry roofs and walls. This will ensure that young chicks which have not developed protective thick feather are protected from UV radiation while the heating of the poultry house is maintained by the heating portion of the electromagnetic spectrum, and as well allows for admittance of VIS light in the house. In comparison, the transmittance of the CNTS film gradually decreases as the film thickness increases and displays an optical transmission over 60% in the near-infrared region. The thinner films of thickness 450 nm show relatively less transparent with transmission about 60%. From these results, it is expected that growingly photons are absorbed in the CNTS films as the thickness is augmented. The drop of transmittance T(λ) with increasing thickness is ascribed probably to the optical scattering and to the boosted free-carrier absorption. This result is in accordance with the fact that the surface roughness of deposited film increases with thickness, which enhances the diffusion and thus a decrease of the transmittance.(Adel *et al*, 2018). The transmittance of thin films can be greatly modified by various growth parameters. In the literature, several authors have reported on the variation of transmittance with parametric investigation involving annealing temperature (Agbo and Nnabuchi, 2011; Augustine and Nnabuchi, 2018), Nnabuchi, 2005.

4.1.3 Reflectance

Figures 7-9 displayed the reflectance curves of Cu_2CoSnS_4, $Cu_2NiSnS4$and Cu_2ZnSnS_4 sensitized thin films. The reflectance spectra of all films exhibited a similar trajectory, fluctuating between maxima and minima (Figs.7-9). Peak reflectance can be observed at 350 nm for Co, Ni and Zn^{2+} doped samples of Cu_2SnS_4, thin films. It can be inferred that the incorporation of dopants concentrations into Cu_2SnS_4 matrix did not significantly affect the reflectance. This suggests that these films layers can be used as antireflective surfaces. The reflectance is generally low suggesting that most of the light were either absorbed or transmitted.

4.1.4 Band gap Energy

The direct band gap of Cu_2CoSnS_4, $Cu_2NiSnS_4$and Cu_2ZnSnS_4 thin films were determined using the intercept of $(\alpha hv)^2$ versus photon energy (hv) plot relying on Tauc's model. Figures 10-12 shows the band gap of doped Cu_2SnS_4 films with Co, Ni and Zn at different concentrates of 0.1 – 0.5M are 1.20eV – 1.30eV for Co^{2+}, 1.25eV – 1.30eV for Ni and 1.25eV – 1.35eV for Zn^{2+} respectively. It was observed that Zn^{2+} concentration showed a slight increase in the band gap energies when compared to Co and Ni ion concentration. This can be attributed to increase in

DOI: https://doi.org/10.57233/ijsgs.v11i2.876 ISSNp: 2488-9229; ISSNe: 3027-1118
IJSGS FUGUSAU VOL. 11(2) WEBSITE: https://fugus-ijsgs.com.ng

energy states as a result of additional layer of the materials. This is in agreement with (Dabajyati and Ramabali, 1987), which state that when spectral absorbance of a film is compared with the bandgap energy which showed that, as the concentration of the ion increases, the energy bandgap decreases. Generally, the wide direct band gap energy exhibited by these films make them ideal for use as window layer in hetero-junction solar cells. The use of wide band gap materials as window layers in solar cell fabrications is to minimize the recombination loss prevalent in direct band gap semiconductors thereby admitting a maximum amount of light to the junction region and the absorber layer. The estimated optical band gap is in line with numerous reports, like; the experimental band gap for the CNTS nanoparticle is estimated to be 1.57eV. The range in the the energy band gap values from 1.25 – 1.3 eV lower the range in values of band gap 1.4 – 1.5eV and 1.0 – 1.5eV obtained for $Cu_2ZnS_nS_4$. For $Cu_2CoS_nS_4$ 1.25-1.30eV and for that of $Cu_2NiS_nS_4$, we have 1.20 – 1.30eV. Thus, we propose CNTS to be a promising candidate for thin-film solar cell applications. (Sachin, *et al*,2017). Cu_2ZnSnS_4 (CZTS) is one of the most promising photovoltaic materials as an alternative absorber layer for the development of low-cost and environmentally friendly thin film solar cells, has a large absorption coefficient of over 10 cm^{-1} with a suitable direct band gap of about 1.5 eV. (Jiahua, *et al*, 2012) . CdS thin films are widely used as window layer in CIGS solar cells. However, there are great concern about the toxicity of Cd in this architecture (Chopra *et al.*, 2004) and so; several alternative window layers are currently being investigated to replace CdS. The values of our band gaps are within the range of direct band gaps reported by other authors for different thin film materials (Augustine and Nnabuchi, 2017), and (Sawanta *et al*, 2012). The wide band gap of 3.54 eV of the films placed them as window materials for solar cell fabrication, high frequency applications as well as in optoelectronics.

4.1.5 Refractive Index

The refractive index of all the thin film samples were very low (n < 0.3) in the NIR. These values of refractive indices are much less than 1.08 and 1.05 values of SiO_2 thin films.

The low values of the refractive indices implied that these kesterites thin films are an excellent absorber of solar radiation and is therefore suitable for photovoltaic application. It is also suitable for other applications in optical devices, such as optical microresonators.

4.1.6 Extinction coefficient

The extinction coefficient (k) is a measure of light loss due to scattering and absorption per unit volume. The plot of extinction coefficient against photon energy for Cu_2CoSnS_4, Cu_2NiSnS_4 and Cu_2ZnSnS_4 thin film are show in figure (17-19). This was found decrease exponentially to the region of fundamental absorption and increase afterward for all the samples. The plot also shows that increasing the doping concentrations gives a significant increase of the extinction coefficient for Cu_2CoSnS_4. In the case of Cu_2NiSnS_4 and Cu_2ZnSnS_4thin films, the extinction coefficient exhibit similar behaviour.

4.1.7 Optical conductivity

The plot of optical conductivity against photon energy for Cu_2CoSnS_4, Cu_2NiSnS_4 and Cu_2ZnSnS_4 thin film are show in figure (20-22). The optical conductivity (σ_{opt}) of the thin films can be calculated using the following relation. [Mali *et al.*, 2014).

$$\sigma_{opt} = \frac{anc}{4\pi} \quad (1)$$

Where n is refractive index, c is speed of light and α is the absorption coefficient. The Optical conductivity σ_{opt} was found to increase with increase in the doping concentration for Cu_2CoSnS_4 thin films. However the trend is not the same for Cu_2NiSnS_4 and Cu_2ZnSnS_4 as their highest optical conductivity occurred at 0.2M and 0.5M respectively.

4.1.8 Real dielectric constant

The physical implication of the dielectric constant is that electromagnetic waves incident on a vacuum can propagate through a sample when the real part is positive, but are totally reflected from the medium when it is negative. This constant is a characteristic property of a given dielectric material, which varies not only from one substance to another but also with the physical state of the material (Pankove, 1971). The dielectric constant (real) characterizes the energy storage of the material and depends on frequency (Agbo, 2014). All the samples recorded very low values (negative value) of real dielectric constant irrespective of the dopant and doping concentrations. The plot show that the real dielectric constant ranges from -1000 to 0 for sample doped with Co and decrease in trend with increase in doping concentration, while real dielectric constant ranges from -1400 to 0 for samples doped with Ni and Zn and decrease also with increase in dopant which is not in trend. A plot of real dielectric Vs hv (eV) were depicted in figures 23 – 25.

4.1.9 Imaginary dielectric constant

The imaginary part (ε_i) of the dielectric constant characterizes the energy dissipation in the material due to relaxation dipole and space charge polarization and due to resonance of ionic and electronic polarization (Agbo, 2014). The imaginary dielectric constant values of all the films vary in a similar pattern (Fig. 26- 28). The imaginary dielectric constant for Cu_2CoSnS_4 ranges from -600 to 0 and increases with increase doping concentrations. Similar trend was exhibited by Cu_2NiSnS_4 and Cu_2ZnSnS_4 thin films. This is a clear indication of the influence of growth parameters on the imaginary dielectric constant of the films. The values of $\varepsilon_{i,}$ are lower in magnitude compared to reported

DOI: https://doi.org/10.57233/ijsgs.v11i2.876 ISSNp: 2488-9229; ISSNe: 3027-1118

IJSGS FUGUSAU VOL. 11(2) WEBSITE: https://fugus-ijsgs.com.ng

values in the Literature (katagiri, et al., 2001; Tanaka et al., 2006). Deposition conditions and other growth variables may have accounted for this behaviour.

5.0 **Morphological Analysis**

The morphology of the various composites were analyzed using Scanning Electron Microscopy (SEM). A scanning electron microscope (SEM) is a type of electron microscope that produces images of a sample by scanning the surface with a focused beam of electrons. The electrons interact with atoms in the sample, producing various signals that reveal information about the sample including external morphology (texture), chemical composition, and crystalline structure and orientation of materials making up the sample. The electron beam is scanned in a raster scan pattern, and the beam's position is combined with the detected signal to produce an image. SEM can achieve resolution better than 1 nanometer (Stokes, Debbie J. 2008).

The structural properties of the **Cu_2SnS_4** thin films doped with Co, Ni and Zn are discussed below.

5.1 Scanning Electron Microsocopy (SEM)

The film microstructure was studied using Scanning Electron Microscopy (SEM). Scanning electron micrographs showed a close packed morphology for all the samples and a decrease in grain size. These were clearly seen in the micrographs for sample doped with Zn. These figures 29 - 34 shows the surface morphological study of Cu_2CoSnS_4, Cu_2NiSnS_4 and Cu_2ZnSnS_4 at (0.1M , 0.3M and 0.5M doping concentrations), it was observed that the grain size of all the samples are larger and more oriented when doped with 0.5M and 0.3M compared to that doped with 0.1M. This means that the average grain size decreased with increase in doping concentrations. Sawanta*et al*, 2012 reported on morphology of Cu_2ZnSnS_4. The report shows an SEM image of the sample CZTS thin film with non-uniform distribution of the agglomerated particles wihin well-defined boundaries. The image shows flake-like morphology compared to ours that are crystalline in nature.

5.2.2 X-ray Diffraction (XRD) pattern

The structures of the Cu_2SnS_4 doped with Co, Ni and Zn thin films were studied using X-ray diffraction (XRD) technique. X-ray diffraction (XRD) patterns were used to identify the crystalline structure of the deposited films. The diffraction spectra were measured at angle 2θ, scanning ranging from 0 to 90 degrees diffraction angle with (CuKα radiation, λ=0.15406 nm). The XRD spectra of Cu_2SnS_4 thin films with slightly different doping concentrations are shown in Figure 35. These patterns show that all films are polycrystalline with hexagonal wurtzite crystal structure. The relative intensities of the peaks increased with increasingin doping concentrations (Ziti *et al.*, 2021). The increase in peak intensities indicates an improvement in the crystallinity of films which is similar to that reported by Rondiya et al, (2017) for Cu_2SnS_4 doped with Nickel, (Chalapathy et al.,2013) for Cu2ZnSnS4 and (Abedi et al., 2020). Intensities of reflections corresponding to the planes samples are different when Zn is incorporated as multiple peaks emerge which is a clear indication that Zn makes compound more crystalline than Co and Ni. The grain size was calculated using Scherrer formula ($\boldsymbol{D = k\lambda/\beta cos\theta}$), where k is a Scherrer's constant taken to be 0.94, λ the wavelength of X-ray used (λ =1.54443Á), D = crystallite size, θ = is Bragg's diffraction angle at peak position and β = is Full width at half maximum of the peak (FWHM) (Lemine, O. M., 2013), was used to estimate the crystallite size from the broadening of the X-ray diffraction peaks.

6.0 CONCLUSION

The kesterite: Cu_2ZnSnS_4, Cu_2NiSnS_4 and Cu_2CoSnS_4, thin films were prepared on glass substrates using Chemical bath deposition (CBD) technique different concentration of 0.1 – 0.5M of , Co^{3+}, Ni^{+} and Zn^{2+} respectively.

These depositions were done at heating water bath temperature of 70°C for a period of 6 hours interval. The grown films were annealed at temperature 200°C.

The synthesis and characterization of the films has shown that dopants like Co^{3+} ,Ni^{+}, Zn^{2+} and temperature improves the optical and structural properties of thin films as observed in our findings.

Conflict of Interest

There are no conflict of interest.

REFERENCES

Adel C., Mohamed F.B., and Brahim B. (2018). Synthesis and Characterization of Photoactive Material Cu_2NiSnS_4 thin films. Journal of Materials Science: Materials in Electronics. Springer Science + Business Media.

Adel H. R, Farahnaz H., Abbas Z .H, Mohammad A. K, Jiri N., Jaroslav M. (2020). Room temperature micro and macro mechanical properties of metastable Ti – 29 Nb – 14 Ta.5Zr alloy holding nano – size precipitates. Journal of Material Science and Engineering, Volume 77.

Agbo, P.E. (2014). Refractive index and Dielectric properties of TiO2/CuO core-shell thin films. Journal of Chemistry and Materials Research, 6(12), 42-45.

Augustine C. and Nnabuchi M.N. (2017). Band gap determination of chemically deposted lead sulphide based heterjunction thin films, Journal of Non-Oxide Glasses, 9(3), 85-98.

DOE (2023). Fossil Energy and Carbon Management US Department of Energy. https://www.energy.gov

DOI: https://doi.org/10.57233/ijsgs.v11i2.876 ISSNp: 2488-9229; ISSNe: 3027-1118

EIA. (2022). Renewable and Nonrenewable Energy. US Energy Information Administration. https://www.eia.gov

Ezema, F.I. (2000). Ph.D Thesis Department of Physics and Astronomy, University of Nigeria, Nsukka.

Habib, M.P., Woo, Y.K., Kwang- Deog, J. and Oh-Shim, J. (2005). A Chemical Route to Room Temperature synthesis of Nanocrystalline TiO2 Thin Films. Applied Surface of Science, 245, 72 – 76.

IEA. (20203). Renewables 2023 International Energy Agency. https://www.iea.org

Islam, R. and Isaacs, N. (2006). Energy used in New Zealand Households – HEEP year 10 Report. Willington BRANZ.

Jinhuo Chen and Li Wenjian (2014). Significant improvement of ZnS film electrical and optical performance by indium incorporation. Journal of semiconductors 35(9)

Lemine O.M, (2013). Synthesis, Structural, Magnetic and Optical properties of nanocrystalline ZnFe2O4. Journal of Physica B:Condensed matter (406) 10 Pp 1989-1994.

Lothion, G.F. (1958). Absorption Spectrophotometery (2nd ed.) Higher and Watts Ltd, London, 345 – 347.

Chattopadhyay, K.K and M.R. (2006). Synthesis and Characterization of Aluminum – doped CdO Thin Films by spray pyrolysis, Solar Energy Materials and Solar Cells,90, 597 – 606.

Mahrov, B.G., Boschloo, Hgfeldt, A., Dloczuk, L. and Dittrich, T. (2004). Photovoltaic study of charge injection from dye molecules into transparent hole and electron conductors. Applied Physics, Lett. 84(26), 5455 – 5447.

Maarja G., Juri K., Charles J.H., Douglas M. B, Oki G. R.S., Samantha M.L., Hannes H., Serglus L and Thomas U.,(2019). The electrical and optical properties of kesterites. Journal of phys Energy, IOP Publishing

Nnabuchi, M. N. (2005). Bandgap and optical properties of chemical bath deposited
magnesium sulphide (MgS) thin films, Pacific Journal of Science and Technology, 6(2), 105-110.

Nnabuchi, M.N. and Augustine, C. (2018). Mn3O4/PbS thin film: Preparation and effect of
annealing temperature on some selected properties, Materials Research Express, 5(3), 1-11.

NREL (2022). Energy Storage National Renewable Energy Laboratory. Hettps://www.nrel.gov

Onah D. U., Ifeanyichukwu B. J., Uguru E. H., Idu H. K. and Ekpe J. E. (2016). Frequency Dependent Electrical Propertis of TiO2/CuO Core-Shell Thin Films. InternationalJournal of Engineering Sciences and Research Technology, 5(2), 386-389.

Ziti H, Idrissi S. Labrium, L Bahmad (2021). Sulfur Doping effect on the electronic properties of Zirconium dioxide ZrO2 , Journal of Material Science and Engineering Volume (27)

World Bank (2021). Financing Renewable Energy. https://www.world bank.org